The following publication H. Guo, B. Sheng, P. Li and C. L. P. Chen, "Multiview High Dynamic Range Image Synthesis Using Fuzzy Broad Learning System," in IEEE Transactions on Cybernetics, vol. 51, no. 5, pp. 2735-2747, May 2021 is available at https://doi.org/10.1109/TCYB.2019.2934823

Multiview High Dynamic Range Image Synthesis Using Fuzzy Broad Learning System

Hongbin Guo, Bin Sheng, Ping Li, Member, IEEE, and C. L. Philip Chen, Fellow, IEEE

Abstract—Compared with the normal low dynamic range (LDR) images, high dynamic range (HDR) images provide more dynamic range and image details. Although the existing techniques for generating HDR images have a good effect for static scenes, they usually produce artifacts on the HDR images for dynamic scenes. In recent years, some learningbased approaches are used to synthesize HDR images and get good results. However, there are also many problems, including the deficiency of explaining and the time-consuming training process. In this paper, we propose a novel approach to synthesize multi-view HDR images through fuzzy broad learning system (FBLS). We use a set of multi-view LDR images with different exposure as input and transfer corresponding Takagi-Sugeno (TS) fuzzy subsystems, then the structure is expanded in a wide sense in the "enhancement groups" which transfer from the TS fuzzy rules with nonlinear transformation. After integrating fuzzy subsystems and enhancement groups with the trained-well weight, the HDR image is generated. In FBLS, applying the incremental learning algorithm and the pseudoinverse method to compute the weights can greatly reduce the training time. In addition, the fuzzy system has better interpretability. In the learning process, IF-THEN fuzzy rules can effectively help the model to detect artifacts and reject them in the final HDR result. These advantages solve the problem of existing deep learning methods. Furthermore, we set up a new dataset of multi-view LDR images with corresponding HDR ground truth to train our system. Our experimental results show that our system can synthesize high-quality multi-view HDR images, which has a higher training speed than other learning methods.

Index Terms—High dynamic range image, fuzzy broad learning system, multi-view synthesis.

I. INTRODUCTION

ITH the rapid demand of information contained in images [2]–[5], HDR images acquisition technique is

Manuscript received March 18, 2019; revised June 24, 2019; accepted August 5, 2019. This work was supported in part by the National Natural Science Foundation of China under Grant 61872241, Grant 61572316, Grant 61751202, Grant 61751205, Grant 61572540, Grant U1813203, and Grant U1801262, in part by the Macau Science and Technology Development Fund under Grant 0027/2018/A1, Grant 079/2017/A2, Grant 024/2015/AMJ, and Grant 0119/2018/A3, in part by the National Key Research and Development Program of China under Grant 2017YFE0104000 and Grant 2016YFC1300302, and in part by the Science and Technology Commission of Shanghai Municipality under Grant 18410750700, Grant 17411952600, and Grant 16DZ0501100.

- H. Guo and B. Sheng are with the Department of Computer Science and Engineering, Shanghai Jiao Tong University, Shanghai 200240, China (e-mail: shengbin@sjtu.edu.cn).
- P. Li is with the Department of Computing, The Hong Kong Polytechnic University, Hong Kong (e-mail: p.li@polyu.edu.hk).
- C. L. P. Chen is with the School of Computer Science and Engineering, South China University of Technology, Guangzhou 510006, China, also with the Navigation College, Dalian Maritime University, Dalian 116026, China, and also with the Faculty of Science and Technology, University of Macau, Macau 999078, China (e-mail: philip.chen@ieee.org).



Tonemapped HDR image







Multi-view LDR images

Fig. 1: Our method uses three different exposure LDR images of the multi-view scene (shown on the bottom) as input and output a high-quality HDR image (shown on the top) via fuzzy broad learning system. Note that, we take the middle exposure LDR image as a reference, then use optical flow method of Liu et al. [1] to align images with low and high exposures to the reference respectively to produce the alignment LDR images. Then use alignment LDR images to synthesize HDR image which contains all of the three LDR images' lighting information through the fuzzy broad learning system.

growing at an explosive speed. The current methods to obtain HDR images are usually divided into two categories: (1) directly capturing with a professional camera, and (2) merging from a set of different exposure LDR images which take from an ordinary digital camera. The former approach can directly obtain high-quality HDR images in dynamic scenes using a professional camera with unique equipment. Nayar et al. [6] placed an optical mask adjacent to a conventional image detector array to sample the spatial and exposure dimensions of image irradiance simultaneously. McGuire et al. [7] used multiple sensors to capture from the same viewpoint but have different image sensors and image parameters simultaneously. Hasinoff et al. [8] proposed noise-optimal capture to capture HDR or reduce noise using the SNR advantage of high ISO settings. Tocci et al. [9] presented an optical architecture for HDR imaging that allows simultaneous capture of high,

© 2019 IEEE. Personal use of this material is permitted. Permission from IEEE must be obtained for all other uses, in any current or future media, including reprinting/republishing this material for advertising or promotional purposes, creating new collective works, for resale or redistribution to servers or lists, or reuse of any copyrighted component of this work in other works.

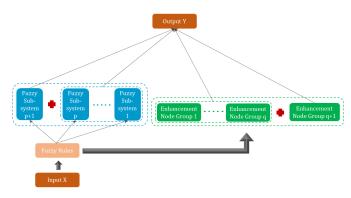


Fig. 2: The structure of increasing fuzzy subsystems and enhancement groups.

medium, and low-exposure images on three sensors. However, these expensive professional hardware result that the former methods could not popularize to the public easily. The second methods such as Debevec et al. [10] and Mann et al. [11] generated well HDR image from LDR images in the static scenes. However, if the scenes are dynamic or the camera is hand-held, these methods produced artifacts like ghosting during the process of aligning in the final HDR image. Therefore, "deghosting" is an important work in the process of synthesizing HDR image. With the development of HDR technology, patch-based approaches of Sen et al. [12] and Hu et al. [13], learning-based approaches of Kalantari et al. [14] and Eilertsen et al. [15] and other approaches of [16]–[21] all get good progress for ghost-free HDR image.

However, existing methods focus on dynamic scenes which are moving or the slight shake of the hand-held camera. They neglect the change of views caused by the movement of the person holding the camera, which produces the multi-view LDR images, for example, as shown in Fig. 1. Thus, we start to work on multi-view HDR synthesis. The essential of synthesizing multi-view HDR is to reduce artifacts produced in the process of aligning. Furthermore, we find that the artifacts can be reduced significantly during the process of synthesizing by detecting artifact regions, which reduces the bad effect in the final HDR result. Thus, we use the learning method to imitate this complex process. Specifically, we use fuzzy broad learning system [22] as our learning model, since IF-THEN fuzzy rules can effectively help the model to detect artifacts and reject them in the final HDR result. This model not only solves the shortcomings of deep learning's long training time but also is interpretable comparing with the traditional deep learning model.

Generally, the process of obtaining final HDR images can be divided into three steps: (1) Align multi-view LDR images to the reference respectively, (2) synthesize the aligned LDR images into an HDR image, and (3) display HDR images after tonemapping. In this paper, we take three multi-view LDR images with high, medium, and low exposures and use the method of Liu et al. [1] to align multi-view LDR images. The LDR images with high and low exposure are aligned to the medium exposure (reference) respectively to obtain three aligned images. In the second step, to eliminate the artifacts

produced during alignment, we adopt the fuzzy broad learning system to synthesize HDR image. In this system, we use the acquired three aligned LDR images as input. We extract features through IF-THEN fuzzy rules to transfer corresponding TS fuzzy subsystems. Simultaneously, the structure is expanded in a wide sense in the enhancement groups which transfer from these extract features with nonlinear transformation to preserve the characteristic of inputs. Therefore, the structure of the system becomes wider instead of deeper. Due to the FBLS's flat network, using pseudoinverse to compute the output-layer weights is a very convenient approach to reduce the training time. Finally, we connect all the fuzzy subsystems and enhancement groups to the output layer with a target weight. In the last step, we need tonemapper since the HDR images could not be displayed on a normal monitor which gray scale is 8 bits. Many powerful tonemapping techniques have been implemented and we choose PhotoshopCS6 to tone map our HDR image. In addition, we retrain the model using incremental learning algorithm through increasing the fuzzy subsystems and enhancement groups. It proves our method is efficient and high-quality. Experimental results demonstrate that our system is correct and efficient. In summary, our approach has the following contributions:

- Multi-view HDR image synthesis Our work proposes a novel research direction on multi-view HDR image synthesis which uses three multi-view LDR images with different exposures. Most existing HDR datasets are captured from static scenes. Some of the datasets lack ground truth images or have a small number of scenes with only rigid motion. In other datasets, the dynamic scenes are caused by the movement of the subject, while the views of different LDR images are the same. As a result, we create the multi-view HDR dataset.
- Using FBLS to synthesize HDR image We adopt fuzzy broad learning system as our learning model. In the learning process, IF-THEN fuzzy rules can effectively help the model to detect artifacts and reject them in the final HDR result. Its efficient, fast and interpretable characteristic produces high-quality HDR result. Due to the flat structure of FBLS, the coefficients in the consequent part of fuzzy rules in every fuzzy subsystem and the weights connecting the final output layer with the outputs of enhancement layer can be computed using pseudoinverse. As a result, compared with deep learning based methods, our method has fast computation nature.
- Incremental learning algorithm for FBLS Our system greatly reduces time as a result of incremental learning, which is a fast remodeling via increasing fuzzy subsystems and enhancement node groups instead of retraining the whole system compared to other learning methods (see Fig. 2). When we increase the number of fuzzy subsystems and enhancement node groups, the new weight matrix can be computed via formerly calculated weights. Thus, we do not have to retrain the whole model, which saves lots of computation time to update the model.

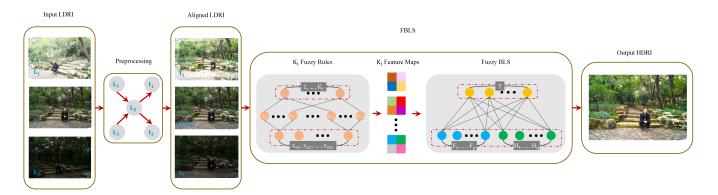


Fig. 3: Overview of the FBLS-HDR synthesis process. We take three multi-view LDR images with different exposures L_1, L_2, L_3 as input data. After preprocessing, we obtain the aligned LDR images. In this step, we use optical flow as our aligned method which use high and low exposure LDR image to align with middle exposure (reference) respectively to generate aligned LDR images I_1, I_2, I_3 . Then, we take I_1, I_2, I_3 as input of FBLS and extract features through K_i fuzzy rules to transform fuzzy subsystems F_i . Simultaneously, the structure is expanded in a wide sense in the enhancement groups H_i which transfer from these extract features with nonlinear transformation to preserve the characteristic of inputs. Finally, we connect all the fuzzy subsystems and enhancement groups to the output layer with a target weight.

II. RELATED WORK

High dynamic range images have received extensive research over the past two decades and acquired a lot of valuable progress. Here, we will introduce the related work about aligning LDR images, rejecting moving object and fuzzy broad learning system respectively.

Align LDR images Greg et al. [23] and Tomaszewska et al. [24] aligned the LDR images through the automatic approaches. Greg et al. [23] used inexpensive shift and difference operations over each image to translate. Tomaszewska et al. [24] used the SIFT algorithm to search for key-points which constitute homography matrices. However, these simpler approaches are unable to use in the dynamic scene. There are also massive alignment algorithms based on optical flow. Bogoni et al. [25] used local unconstrained motion estimation to align the LDR images. Myszkowski et al. [26] used optical flow to compute a dense motion field that formed a local correction to the global transformation and then merged HDR images by rejecting the pixel which was not corresponding to the reference. Mangiat et al. [27] performed simpler block-based motion estimation and refined the motion vectors using color similarity in the adjacent frames. In [28], HDR images were aligned with the energy-based optical flow which minimizes an energy function of the data term on the gradient constancy assumption and smoothness term. Hu et al. [13] presented a displacement estimation method based on generating a perfectly aligned image which successfully deals with large saturated regions in the reference image. However, the state-of-the-art alignment algorithms using optical flow in the challenging scenes also produce artifacts on the final HDR image.

Reject moving object Rejecting moving object is another important work for synthesizing HDR images. These approaches identify and reject the moving object to avoid generating ghost. Liu et al. [29] used advanced CMOS image sensors to capture multiple images within a normal exposure time to reject ghost. Grosch et al. [30] predicted the pixel color

from one image to another using camera response function and the difference between the two colors which indicated object motion. Gallo et al. [16] and Raman et al. [31] did the similar approach with Grosch et al. [30]. Khan et al. [32] and Heo et al. [17] did not require explicit object detection and motion estimation. Khan et al. [32] iteratively weighted each pixel according to its probability of belonging to the background. Heo et al. [17] utilized the global intensity transfer functions which obtained from joint probability density functions between different exposure images and weighted each exposure according to the Gaussian-weighted distance to a reference value. Jacobs et al. [33] detected motions which used the difference in local entropy between different exposure images. Jinno et al. [34] used Markov random field [35], [36] to estimates displacements, occlusion as well as saturated regions, and reject motion blur. Sidibe et al. [37] proposed a detection for ghosting region via an order relation between pixel values in consecutive images.

3

Min et al. [38] proposed a histogram based ghost removal method, in which object motion and background change between two exposures were detected using multi-level thresholding of the intensity histogram. Pece et al. [39] used the median threshold bitmap algorithm to generate bitmaps for each exposure image and detected movement when the value changes in a pixel. Wu et al. [40] proposed three criterions of monotonous, pixel error and color error to detect the moving objects. Zhang et al. [41] utilized the gradient direction changes to reveal object movement. Sen et al. [12] proposed a novel patch-based energy-minimization formulation that integrates alignment and reconstruction in a joint optimization through an HDR image synthesis equation. Based on Sen's patch-match method, Kalantari et al. [42] proposed HDR video generation using alternate exposures in 2013 and used deep learning to reject artifact in 2017 [14] which was the first learning method in HDR field. Granados et al. [43] proposed a method that models the noise distribution of color values

and used a Markov random field to reconstruct irradiance from pixels that were likely to correspond to the same static scene object. Lee et al. [19] assumed that irradiance maps were linearly related to low dynamic range image exposures and formulated ghost region detection as a rank minimization problem by restricting moving objects. Oh et al. [44] improved Lee's method that handled moving objects with large overlapping area.

Fuzzy Broad learning system Before understanding fuzzy broad learning, we firstly introduce the deep learning and broad learning respectively. Deep learning is a new field in machine learning research [45]-[48], and it has a wide range of applications in image processing, speech recognition, and large-scale data processing [49]–[52]. Deep belief network (DBN) was one of the earliest neural networks. Hinton et al. [53] proposed restricted Boltzmann machines which can be stacked and trained in a greedy manner to form a deep belief network. Convolutional neural network (CNN) [54] is the most popular neural network. Kalantari et al. [14] used CNN as a learning model and compared three different architectures which output estimated HDR image, blending weights and refined aligned to merge HDR images respectively. Although they presented high-quality results, they suffered too long training time. Single layer feed forward neural (SLFN) network has been widely used in many fields for its good learning ability [55], [56]. However, it has slow training speed, which easily falls into local minima and could not reach the global minimum. The random vector functional-link neural network (RVFLNN) [56], [57] effectively eliminated the drawback of the long training process. However, it could not do well on large-scale data and time-variety. Chen et al. [58] proposed a fast learning algorithm which found optimal weights of the flat neural networks. Based on the work in [58], broad learning system (BLS) [59], [60] was proposed. The feature nodes and enhancement nodes from input data were integrated into the output and the incremental learning algorithm can remodel the architecture through increasing input data, feature nodes, and enhancement nodes without retraining original architecture.

In the study of past fuzzy systems, the network based on a set of IF-THEN fuzzy rules of fuzzy system with the learning and connecting structure of neural network which named fuzzy neural network (FNN) achieved a lot of excellent results. However, the FNN follows the neural network's training method to train the parameters in the fuzzy rules and cost much time. Due to the massive data and big dimension, fuzzy rules' accuracy choice is a problem. To solve these problems, many improved approaches have been proposed recently. Wang et al. [61] proposed a novel hierarchical hybrid fuzzy neural network which the fuzzy sub-systems aggregates several discrete input variables into an intermediate variable and neural network rest consist of continuous input variables and intermediate variables. Hai et al. [62] proposed an online sequential fuzzy extreme learning machine (OS-Fuzzy-ELM), its learning can be done with the input data coming in a one-by-one mode or a chunk-by-chunk mode with and randomly assigned all the antecedent parameters of membership functions to cut down the learning time. Zhan et al. [63] proposed a neurofuzzy inference system which grouped the data by the k-means

Algorithm 1 Synthesis HDR Image Using FBLS

Input: Aligned Images I, fuzzy rules K_i , fuzzy subsystems p, enhancement node groups qOutput: Final HDR Image 1: Take X = I; 2: Random the parameter α_{kt}^i in [0,1]; 3: **for** i = 1; i <= p **do for** s = 1; s <= n **do** Calculate Z_{si} using Eq. (4); 5: Calculate F_{si} using Eq. (9); 6: 7: Obtain the Z_i using Eq. (5); 8: 9: Obtain the F_i using Eq. (10); 10: end for 11: Obtain Z^p using Eq. (6); 12: **for** j = 1; j <= q **do** Randomly generated ω_i, β_i ; 13: Calculate H_i using Eq. (7); 15: end for 16: Obtain the enhancement node groups H^q using Eq. (8); 17: Obtain the fuzzy subsystems F^p using Eq. (11); 18: Use trained well weight W to generate final HDR image with Eq. (12);

clustering method and the membership of arbitrary input for each fuzzy rule was derived through an ELM. However, they only consider one fuzzy system in their models. Recently, Feng et al. [22] proposed a fuzzy learning model based on broad learning system which includes fuzzy subsystems and enhancement groups.

III. APPROACH FRAMEWORK

In our proposed method, we use a set of multi-view LDR images with different exposures (L_1, L_2, L_3) to synthesize high-quality HDR images (H) with little ghost via FBLS (see Algorithm 1). In the alignment stage, we regard the middle exposure image (L_2) as the reference, then align low exposure image (L_1) and high exposure image (L_3) to the reference (the middle exposure) using optical flow method of Liu et al. [1], respectively. The new generated aligned images with different exposures are denoted as $I = \{I_1, I_2, I_2\}$. The most advanced algorithm which used optical flow to align the LDR images could not work accurately and produce ghosting artifacts in some complex motions. To reduce the influences of this phenomenon on the final HDR images, we proposed to generate HDR image using fuzzy broad learning system. In the training step, we take the aligned image I_1 , I_2 , I_3 and the ground truth as input, output the connection weight. In the testing step, we input the aligned image I_1 , I_2 , I_3 and output our HDR result. The process of synthesizing multi-view HDR image is shown in Fig. 3. In some cases, if the quality of the final HDR image quality could not reach our expectation, we need incremental learning to proceed to refine our learning model. We describe the HDR synthesis system in Section IV and interpret the incremental learning in Section V.

IV. GENERATE HDR IMAGE

A. Preprocessing

If the format of the multi-view LDR images is not RAW, we use camera response curve in [10] to linearize them. Then we use gamma curve $(\gamma=2.2)$ on these linear images to obtain LDR images (L_1,L_2,L_3) suitable for our method. This step makes the LDR images closer to the real. Before aligning, we need to adjust exposure of the reference image (L_2) to high exposure image L_3 and adjust low exposure image L_1 to the reference image L_2 , respectively, since the optical flow methods require brightness constancy. Formally, it is denoted as: $L^{1,2} = clip(L_1exposure(L_1,L_2)^{\frac{1}{\gamma}})$ and $L^{2,3} = clip(L_2expourse(L_2,L_3)^{\frac{1}{\gamma}})$, where exposure(1) is the exposure ratio between the reference and the low or high exposure. Then we use optical flow method in [1] to compute the flow between L_1 and $L^{1,2}$, and the flow between L_3 and $L^{2,3}$ to obtain the aligned images $I = \{I_1,I_2,I_2\}$.

B. HDR Synthesis

In this step, we use the aligned images I as input of FBLS $\mathbf{X} = (\mathbf{x}_1, \mathbf{x}_2, \dots, \mathbf{x}_n)^T \in \mathbb{R}^{n \times m}$ and output the HDR image. At first, we use first-order TS fuzzy model to map the input $\mathbf{x}_s = (x_{s1}, x_{s2}, \dots, x_{sm})$ to the ith fuzzy system. In first-order TS fuzzy model, the function of x_{st} is first order polynomial, where $t = 1, 2, \dots, m$. This can be defines as:

$$z_{sk}^i = \sum_{t=1}^m \alpha_{kt}^i x_{st} \tag{1}$$

where α_{kt}^i is a parameter generated randomly and $k=1,2,\ldots,K_i$ is the number of fuzzy rule of the *i*th fuzzy system. We adopt Gaussian membership function as our membership function, this can be denoted as:

$$\mu_{kt}^{i}(x_{st}) = e^{-\left(\frac{x_{st}^{i} - c_{kt}^{i}}{\sigma_{kt}^{i}}\right)^{2}}$$
 (2)

where c_{kt}^i are centers of the Gaussian membership functions and the width σ_{kt}^i is a fixed value. We use classic k-means method on the training data to obtain K_i clustering centers. The values of c_{kt}^i are decided by these clustering centers. Then, the weighted activation level for each rule can be computed as:

$$\omega_{sk}^{i} = \frac{\prod_{t=1}^{m} \mu_{kt}^{i}(x_{st})}{\sum_{k=1}^{K_{i}} \prod_{t=1}^{m} \mu_{kt}^{i}(x_{st})}$$
(3)

After the above calculation, the intermediate output \mathbf{Z}_{si} for the sth training sample of the ith fuzzy subsystem can be denoted as:

$$\mathbf{Z}_{si} = (\omega_{s1}^{i} z_{s1}^{i}, \omega_{s2}^{i} z_{s2}^{i}, \dots, \omega_{sK_{i}}^{i} z_{sK_{i}}^{i}) \tag{4}$$

the intermediate output \mathbf{Z}_i for all the training samples of the ith fuzzy subsystem can be denoted as:

$$\mathbf{Z}_i = (\mathbf{Z}_{1i}, \mathbf{Z}_{2i}, \dots, \mathbf{Z}_{ni}), i = 1, 2, \dots, p.$$
 (5)

then the intermediate output \mathbf{Z}^p of p fuzzy subsystems can be denoted as

$$\mathbf{Z}^p = (\mathbf{Z}_1, \mathbf{Z}_2, \dots, \mathbf{Z}_p) \in \mathbb{R}^{n \times (K_1 + K_2 + \dots + K_p)}$$
 (6)

Then, we enhance the intermediate output to the enhancement node groups, this can be defined as:

$$\mathbf{H}_{j} = \psi(\mathbf{Z}^{p}\boldsymbol{\omega}_{j} + \boldsymbol{\beta}_{j}), \quad j = 1, 2, \dots, q$$
 (7)

5

where \mathbf{H}_j is the enhancement groups transformed from \mathbf{Z}^p , which can preserve the characteristic of inputs. ω_j and β_j are weight and bias randomly generated from [0,1] with proper dimensions which transform \mathbf{Z}^p to \mathbf{H}_j . $\psi(\cdot)$ is a activation function which use Sigmoid function. And all the enhancement node groups are denoted as:

$$\mathbf{H}^q = (\mathbf{H}_1, \mathbf{H}_2, \dots, \mathbf{H}_q) \tag{8}$$

The output vector \mathbf{F}_{si} for the sth training sample of the ith fuzzy subsystem consists of z_{sk}^i . To avoid the computational complexity, we do not compute the coefficient α_{kt}^i in pseudoinverse explained in Eq. 13, but introduce a new parameter λ_{kc}^i . It can be defined as:

$$\mathbf{F}_{si} = \left(\sum_{k=1}^{K_i} \lambda_{k1}^i \omega_{sk}^i z_{sk}^i, \dots, \sum_{k=1}^{K_i} \lambda_{kC}^i \omega_{sk}^i z_{sk}^i\right)$$

$$= \left(\sum_{k=1}^{K_i} \lambda_{k1}^i \omega_{sk}^i \left(\sum_{t=1}^m \alpha_{kt}^i x_{st}\right)\right), \dots,$$

$$\left(\sum_{k=1}^{K_i} \lambda_{k1}^i \omega_{sk}^i \left(\sum_{t=1}^m \alpha_{kC}^i x_{st}\right)\right)$$

$$= \sum_{t=1}^m \alpha_{kt}^i x_{st}(\omega_{s1}^i, \dots, \omega_{sK_i}^i) \begin{pmatrix} \lambda_{11}^i & \dots & \lambda_{1C}^i \\ \vdots & & \vdots \\ \lambda_{K_i}^i & \dots & \lambda_{K_iC}^i \end{pmatrix}$$
(9)

where c = 1, 2, ..., C. The output matrix \mathbf{F}_i for all the training samples of the *i*th fuzzy subsystem is denoted as:

$$\mathbf{F}_i = (\mathbf{F}_{1i}, \mathbf{F}_{2i}, \dots, \mathbf{F}_{ni}) = \mathbf{D}\mathbf{\Omega}^i \boldsymbol{\lambda}^i$$
 (10)

where $\mathbf{D} = diag\{\sum_{t=1}^{m} \alpha_{kt}^i x_{1t}, \dots, \sum_{t=1}^{m} \alpha_{kt}^i x_{nt}\}$, and

$$oldsymbol{\Omega}^i = egin{pmatrix} \omega^i_{11} & \dots & \omega^i_{1K_i} \ dots & \dots & dots \ \omega^i_{n1} & \dots & \omega^i_{nK_i} \end{pmatrix}, \ oldsymbol{\lambda}^i = egin{pmatrix} \lambda^i_{11} & \dots & \lambda^i_{1C} \ dots & \dots & dots \ \lambda^i_{K_i1} & \dots & \lambda^i_{K_iC} \end{pmatrix}.$$

Let \mathbf{F}^p denote the aggregative output of p fuzzy subsystems, written as:

$$\mathbf{F}^{p} = \sum_{i=1}^{p} \mathbf{F}_{i} = \sum_{i=1}^{p} \mathbf{D} \mathbf{\Omega}^{i} \boldsymbol{\lambda}^{i} = \mathbf{D}(\mathbf{\Omega}^{1}, \dots, \mathbf{\Omega}^{p}) \begin{pmatrix} \boldsymbol{\lambda}^{1} \\ \vdots \\ \boldsymbol{\lambda}^{p} \end{pmatrix} = \mathbf{D} \mathbf{\Omega} \boldsymbol{\Lambda}$$
(11)

where $\Omega=(\Omega^1,\ldots,\Omega^p)$ and we denote $((\lambda^1)^T,\ldots,(\lambda^p)^T)^T$ as Λ .

Finally, we connect the fuzzy subsystems \mathbf{F}^p and the enhancement node groups \mathbf{H}^q to the output \mathbf{Y} . The weights connecting to the output of \mathbf{F}^p and \mathbf{H}^q are \mathbf{W}_f and \mathbf{W}_h ,

respectively. Hence, the fuzzy broad learning system model can be denoted as:

$$\mathbf{Y} = \mathbf{F}^{p} \mathbf{W}_{f} + \mathbf{H}^{q} \mathbf{W}_{h}$$

$$= \mathbf{D} \mathbf{\Omega} \mathbf{\Lambda} + \mathbf{H}^{q} \mathbf{W}_{h}$$

$$= (\mathbf{D} \mathbf{\Omega}, \mathbf{H}^{q}) \begin{pmatrix} \mathbf{\Lambda} \\ \mathbf{W}_{h} \end{pmatrix}$$

$$= \mathbf{A} \mathbf{W}$$
(12)

where $\mathbf{A} = (\mathbf{D}\Omega, \mathbf{H}^q)$ and the values of the weights \mathbf{W}_f are set to be 1. $\mathbf{W} = \begin{pmatrix} \mathbf{\Lambda} \\ \mathbf{W}_h \end{pmatrix}$ is the final connecting weight matrix of the FBLS. The weight matrix \mathbf{W} can be computed using the training targets $\mathbf{Y} : \mathbf{W} = \mathbf{A}^+ \mathbf{Y}$.

The pseudoinverse matrix \mathbf{A}^+ could be obtained by the optimization problem:

$$\mathbf{A}^{+} = \arg\min_{\mathbf{W}} \|\mathbf{A}\mathbf{W} - \mathbf{Y}\|_{2}^{2} + \lambda \|\mathbf{W}\|_{1}$$
 (13)

We use a improved least square to obtained the connecting weight \mathbf{W} with smallest training errors, and λ denote the further constraints on the sum of the squared weights in [59]. The first terms is a l_2 norm regularization which denotes the training errors. The second term is a a l_1 norm regularization which prevents our model from over fitting. Obviously, we could obtain $\mathbf{W} = (\lambda \mathbf{E} + \mathbf{A} \mathbf{A}^T)^{-1} \mathbf{A}^T \mathbf{Y}$, where \mathbf{E} is a unit matrix. If $\lambda \to 0$, we have: $\mathbf{A}^+ = \lim_{\lambda \to 0} (\lambda \mathbf{E} + \mathbf{A} \mathbf{A}^T)^{-1} \mathbf{A}^T$. Overall, in this step, we can synthesize the HDR image using the trained well weight matrix \mathbf{W} in the FBLS system.

V. OPTIMIZATION OF TRAINING RESULT

In other deep learning models, if the learning effect does not work well as expected, they will increase the number of the filter or increase the number of the layer, which needs to retrain the new network for a long time. In our FBLS, we can increase additional enhancement node groups and fuzzy subsystems to reconstruct the model using an incremental learning algorithm without the process of retraining the whole system (see Algorithm 2). It has better performance. We use PSNR to evaluate the accuracy of our HDR results. If the PSNR value of the final HDR images is less than 40, we need to increase the enhancement node group and fuzzy subsystem to raise our HDR result's quality. We denote the additional enhancement node group as $\mathbf{H}_{q+1} = \psi(\mathbf{Z}^p \cdot \boldsymbol{\omega}_{q+1} + \boldsymbol{\beta}_{q+1}),$ where ω_{q+1} , β_{q+1} are weight and bias generated randomly from fuzzy subsystems to the additional enhancement node group with proper dimensions. And the new matrix after increasing additional enhancement node group is denoted as \mathbf{A}^{q+1} :

$$\mathbf{A}^{q+1} = [\mathbf{A} \mid \mathbf{H}_{q+1}] \tag{14}$$

Then we calculate the pseudoinverse of the new matrix (\mathbf{A}^{q+1}) as:

$$(\mathbf{A}^{q+1})^{+} = \begin{bmatrix} \mathbf{A}^{+} - (\mathbf{A}^{+}\mathbf{H}_{q+1})\mathbf{B}^{T} \\ \mathbf{B}^{T} \end{bmatrix}$$
(15)

where **B** is detailed explanation in [59].

Finally, the dynamic updating weight \mathbf{W}^{q+1} can be calculated by :

$$\mathbf{W}^{q+1} = \begin{bmatrix} \mathbf{W} - (\mathbf{A}^{+}\mathbf{H}_{q+1})\mathbf{B}^{T}\mathbf{Y} \\ \mathbf{B}^{T}\mathbf{Y} \end{bmatrix}$$
(16)

Algorithm 2 Incremental Learning Algorithm

15: until The PSNR value is satisfied

16: Update connecting weight;

```
Output: Dynamic updated connecting weight
 1: repeat
       if increase the enhancement group then
 2:
 3:
           Randomly generated \omega_{q+1} and \beta_{q+1};
           Calculate new enhancement node group H_{q+1} =
    \psi(Z^p\omega_{q+1}+\beta_{q+1});
           Set the new matrix A_{q+1} using Eq. (14);
           Update (A^{q+1})^+ using Eq. (15);
 7:
            Update connecting weight W^{q+1} using Eq. (16);
 8:
       end if
 9:
       if increase the fuzzy subsystem then
           Calculate new fuzzy subsystem F_{p+1}
11:
           Set the new matrix A_{p+1};
           Update (A_{p+1})^+ using Eq. (18);
12:
           Update connecting weight W^{p+1} using Eq. (19);
13:
14:
       end if
```

Input: Training samples (X, Y), original connecting weight

Only increase the enhancement nodes may also not satisfy our quality requirements, because the feature mapping of fuzzy subsystem we extract may not completely include the whole features of the input data. Therefore, we can increase the number of fuzzy subsystems to improve quality. We denote the additional fuzzy subsystem as \mathbf{F}_{p+1} :

$$\mathbf{F}_{p+1} = \mathbf{D}\mathbf{\Omega}^{p+1}\lambda^{p+1} \tag{17}$$

We denoted the new matrix as $\mathbf{A}^{p+1} = [\mathbf{A} \mid \mathbf{D}\Omega^{p+1}]$. Then we calculate the pseudoinverse $(\mathbf{A}^{p+1})^+$ similar to Eq.15 and the dynamic updating weight \mathbf{W}^{p+1} similar to Eq.16:

$$(\mathbf{A}^{p+1})^{+} = \begin{bmatrix} \mathbf{A}^{+} - (\mathbf{A}^{+}\mathbf{D}\mathbf{\Omega}^{p+1})\mathbf{B}^{T} \\ \mathbf{B}^{T} \end{bmatrix}$$
(18)

$$\mathbf{W}^{p+1} = \begin{bmatrix} \mathbf{W} - (\mathbf{A}^{+} \mathbf{D} \mathbf{\Omega}^{p+1}) \mathbf{B}^{T} \mathbf{Y} \\ \mathbf{B}^{T} \mathbf{Y} \end{bmatrix}$$
(19)

Overall, due to our model's flat structure, we can increase fuzzy subsystems and enhancement node groups through pseudoinverse to avoid retraining the whole model.

VI. EXPERIMENTAL RESULTS

In this section, in order to prove that our proposed method is efficient and generates a high-quality result, we will show the experiment in four parts, including datasets and implementation, evaluation, comparisons and running time.

A. DataSets and Implementation Details

DataSets In order to train our FBLS to have a better performance without artifacts, we need a large dataset which consists of the multi-view LDR images with different exposure and the corresponding ground truth. However, there is no such existing dataset. Therefore, we create a new dataset of multi-view HDR synthesis which includes a set of 100 training

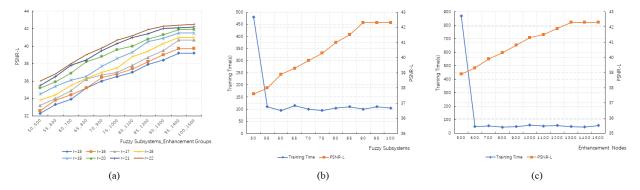


Fig. 4: Parameter analysis experiment. We keep the remain parameters in our defined value and adjust some parameters in each experiment. (a) Experiment of increasing the fuzzy rules and fuzzy subsystem-enhancement group. (b) Experiment of increasing the fuzzy subsystems from 50 to 100 to observe the PSNR-L and the training time simultaneously. (c) Experiment of increasing the enhancement nodes from 500 to 1500 to observe the PSNR-L and the training time simultaneously.

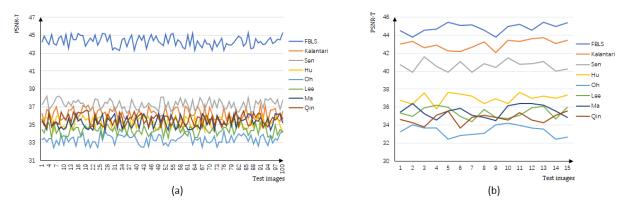


Fig. 5: Compare the values of PSNR-T with state-of-the-art methods (Hu et al. [13], Sen et al. [12], Qin et al. [20], Ma et al. [21], Lee et al. [19], Oh et al. [44] and Kalantari et al. [14]) on our multi-view test set and Kalantari [14] test set (deep learning method) respectively. (a) Test on 100 scenes of our multi-view test set. (b) Test on 15 scenes of Kalantari test set.

scenes and 100 test scenes, each set of the scene contains 3 different exposure multi-view LDR images in .tif format with its corresponding ground truth image in .hdr format. The training scenes contain indoor, outdoor, sunny day and cloudy day. The resolution of these images is 1500*1000 and the exposure biases of LDR images is (-2.0,0.0,2.0). Note that, we use the approach of Kalantari et al. [14] to generate the corresponding ground truth HDR image.

Implementation Details We implement our approach using MATLAB on a laptop with 4.00-GHz Intel i7 CPU, 32GB memory. We use the set of 100 scenes as our training data. We set the randomly generated weights in the enhancement node groups ω_j and β_j within the interval of (-1,1), the coefficients α_{kt}^i are initialized randomly in (0,1). In addition, we set the parameter λ for ridge regression in Eq. (13) as 10^{-6} and set the σ_{kt}^i in Eq. (2) as 1. The activation function which transforms the enhancement node groups is nonlinear sigmoid functions. For setting the number of fuzzy subsystems, enhancement node groups and fuzzy rules, in the beginning, we set the number of fuzzy rules as 15, fuzzy subsystems as 50 and enhancement nodes as 500, then we respectively increase the amount of fuzzy subsystems from 50 to 100, and enhancement nodes from 500 to 1500 to retrain

our model. Simultaneously, we observe the variety of PSNR-T (computed using tonemapped outputs and ground truth) and PSNR-L (computed using linear images and ground truth) to obtain the optimal model parameters. Then we increase the number of fuzzy rules from 15 to 25 to adjust our model while keeping the number of fuzzy subsystems and enhancement nodes are constant. Finally, we set the number of fuzzy subsystems as 90, the number of enhancement groups as 1300 and the number of fuzzy rules as 22, which can obtain the highest quality HDR image and cost the least time relatively. If we keep on increasing the number of fuzzy subsystems, enhancement nodes and fuzzy rules, the quality of the result have little improved and also cost much time. This parameter analysis experiment is shown in Fig. 4. From Fig. 4(b) and Fig. 4(c), we can see that the training time has a large decline when increasing the number. It proves that we do not need to retrain the whole model when increasing the fuzzy subsystems and enhancement nodes.

7

B. Evaluations

In this section, we compare our method with state-of-theart methods, including two based patch method [12], [13],

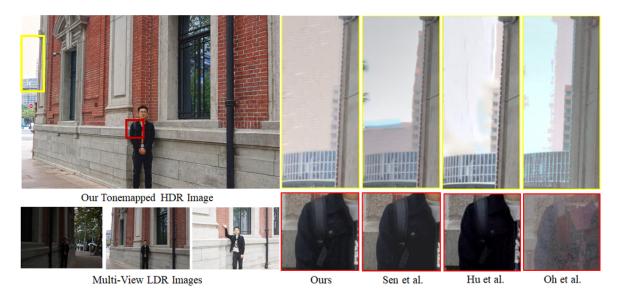


Fig. 7: Compare the HDR results on *man1* of our multi-view dataset with the state-of-the-art methods of Sen et al. [12], Hu et al. [13] and Oh et al. [44].



Fig. 9: Compare HDR results on *man3* of Kalantari's dataset with the state-of-the-art methods of Kalantari et al. [14], Eilertsen et al. [15], Sen et al. [12], Hu et al. [13] and Oh et al. [44].

a deep learning CNN method [14] and a motion rejection method [44]. All the results are implemented by the authors' improved code. In order to prove our method has better performance, we make quantitative evaluation using PSNR-T, PSNR-L and HDR-VDP-2 [64] which is a calibrated visual metric for visibility and quality prediction for HDR images on 15 scenes of Kalantari's test set [14]. Note that, there is no training data used in the test data. The higher average value of three kinds of metric method denotes which is more similar to the ground truth. From Table I, we can see that our values of PSNR-T and PSNT-L are higher than the state-of-the-art methods, which means our proposed method better restores the real scene detail. Kalantari's method obtains the highest HDR-VDP-2 score. We also compare the values of PSNR-T on 100 scenes of our multi-view test set and 15 scenes of Kalantari's test set with state-of-the-art methods (Hu et al. [13], Sen et al. [12], Qin et al. [20], Ma et al. [21], Lee et

TABLE I: Quantitative results of three metric method

Kalantari's Dataset	Method							
Kalalitali S Dataset	Sen [12]	Hu [13]	Oh [44]	Kalantari [14]	Ours			
PSNR-T	40.70	35.53	32.27	42.72	43.24			
PSNR-L	37.98	30.81	34.37	41.20	42.33			
HDR-VDP-2	63.85	60.74	61.28	64.03	63.51			

al. [19], Oh et al. [44] and Kalantari et al. [14]) in Fig. 5. The row coordinates are different test images. From the figure we can see, our FBLS has better performance on both two test sets. It indicates our proposed can produce high quality HDR results not only on the multi-view but on the traditional dynamic scenes. However, other approaches are not able to apply in our multi-view scenes. In addition, we evaluate the stability of our model. We set the enhancement nodes as 1500 and test our model with increasing of fuzzy rules and fuzzy subsystems. From Fig. 6 we can see, the values of PSNR-L are rising generally. It shows that our model is stable.

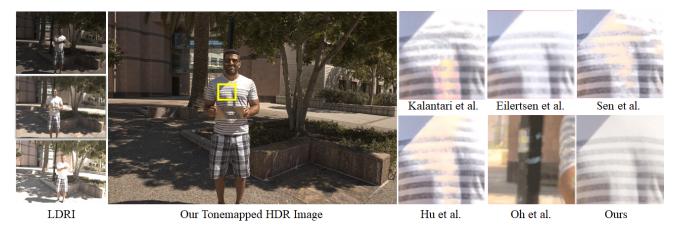


Fig. 10: Compare HDR results on *man4* of Kalantari's dataset with the state-of-the-art methods of Kalantari et al. [14], Eilertsen et al. [15], Sen et al. [12], Hu et al. [13] and Oh et al. [44].

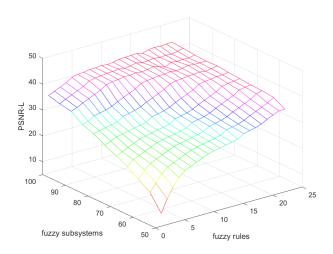


Fig. 6: With the fuzzy subsystems and fuzzy rules increasing, the values of PSNR-L are on the rise on the whole. It confirms the stability of our system.

C. Comparisons

We compare our method on our multi-view test data with state-of-the-art methods of Sen et al. [12], Hu et al. [13] and Oh et al. [44] which is shown in Fig. 7 and Fig. 8. In the left of each figure is the three multi-view LDR images with different exposures and the middle is the reference. Figure 7 shows a man on the street on a cloudy day. In the red block, Oh et al. [44] are not able to avoid alignment artifacts caused by the significant multi-view motions. And in the dark region, Hu et al. [13] are not able to recover the detail of the black clothes. In the yellow block of the building in the distance, Oh et al. [44] still produce a lot of alignment artifacts, Hu et al. [13] produce blur and Sen et al. [12] generate both alignment artifacts as well as blur. Our method can synthesize a blurfree and artifact-free high-quality HDR result. Figure 8 shows a man in the green park on a cloudy day. In the red block, other approaches are not able to avoid alignment artifacts (Oh et al. [44]), could not recover the highlight (Sen et al. [12])

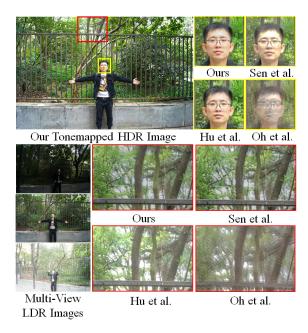


Fig. 8: Compare HDR results on *man2* of our multi-view dataset with the state-of-the-art methods of Sen et al. [12], Hu et al. [13] and Oh et al. [44].

and produce blur in the whole image (Hu et al. [13]). In the yellow block, the approach of Hu et al. [13] could not recover the highlight of the sky behind the leaves. The approach of Sen et al. [12] produces blur around the tree and the approach of Oh et al. [44] generates serious artifacts. In contrast, our result has better performance.

We compare our method on Kalantari's dataset [14] with the state-of-the-art methods of Kalantari et al. [14], Sen et al. [12], Hu et al. [13], Oh et al. [44] and Eilertsen et al. [15], which is shown in Fig. 9 and Fig. 10. In Fig. 9, because of the significant foreground motions of the people, the patch-based approaches (Sen et al. [12], and Hu et al. [13]) produce a lot of artifacts around the moving region. In contrast, the learning-based approaches (Kalantari et al. [14], Eilertsen et

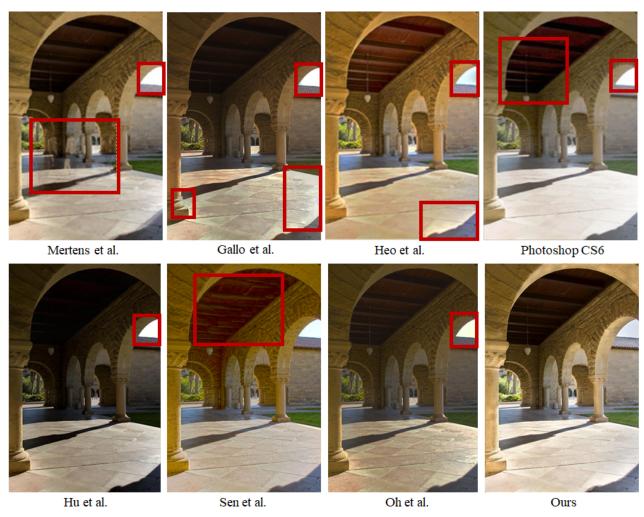


Fig. 11: Compare HDR results on *arch* of Gallo's [16] dataset with the state-of-the-art methods of Mertens et al. [18], Gallo et al. [16], Heo et al. [17], Photoshop CS6, Hu et al. [13], Sen et al. [12] and Oh et al. [44].

al. [15] and ours) produce better results. However, the result of Kalantari et al. [14] also has some artifacts and the result of Eilertsen et al. [15] produce saturated highlights and blur. Our approach is able to produce a high-quality HDR image with little artifacts and highlights. Similarly, in Fig. 10, in the highly saturated highlight regions, the result of Kalantari et al. [14], Sen et al. [12], Hu et al. [13] and Oh et al. [44] produce a lot of artifacts. The result of Eilertsen et al. [15] is better but still has a little blur. Our results are able to hallucinate plausible details in saturated regions.

We compare our method on Gallo's dataset [16] with state-of-the-art methods shown in Fig. 11 and Fig. 12. The ArchSequence in Fig. 11 consists of five different exposure LDR images, we choose three of them to test our proposed method with exposure value (-2.0,0.0,2.0). In Fig. 11, the result of Mertens et al. [18] has an obvious ghost of moving person, because they do not align the dynamic scenes and just handle the static scenes. In the lower left corner and lower right corner of Gallo et al. [16], their result produces blur and saturated highlights respectively. The result of Heo et al. [17] and Photoshop CS6 generated halo artifacts and blending artifacts respectively. The patch-based result of Hu et

al. [13] and Sen et al. [12] produce blur and noise in the dark regions since they preserved information from the reference heavily. These results all reject ghost successfully in addition to Mertens et al. [18]. The result of Oh et al. [44] and most of these results are not able to recover the sky. Our method shows more details and high quality of the scenes especially. In Fig. 12, we compare our result with Gallo et al. [16], Hu et al. [65] and Hu et al. [13]. In the red block which is bright region, our result and Gallo's have better performance, however, Hu et al. [65] and Hu et al. [13] produce highlight. On the contrary, in the yellow block which is dark region, Gallo et al. [16] did not restitute detail of the scene and the tree stump contained some blur. Moreover, compared to our method in the blue block, other methods have different degrees of blur.

D. Running Time

In order to prove our proposed approach is efficient, we compare the execution time with Hu et al. [13], Sen et al. [12], Oh et al. [44], Kalantari et al. [14] and Lee et al. [19] on 6 scenes from different dataset in Table II. From Table II, we can see our running time is much less than Sen et al. [12] and Hu et al. [13], and close to the running time of

Scenes	Image Size	Sen et al. [12]	Hu et al. [13]	Lee et al. [19]	Oh et al. [44]	Kalantari et al. [14]	FBLS
		MATLAB+Mex	MATLAB+Mex	MATLAB+Mex	MATLAB	MATLAB+Mex	MATLAB
man1	1500×1000	210.28	314.96	106.91	120.93	113.78	122.41
man2	1500×1000	237.52	332.34	115.35	108.41	106.12	131.53
man3	1500×1000	242.19	340.13	136.39	140.03	124.65	103.96
man4	1500×1000	205.57	338.70	121.27	129.14	119.76	116.72
arch	699×1024	95.38	154.96	56.24	70.33	52.04	60.39
forrest	1024×683	159.28	213.27	82.46	91.40	83.20	79.15

TABLE II: Compare runtime in seconds

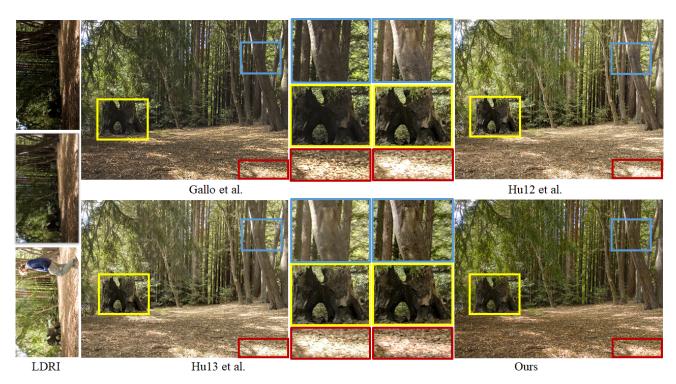


Fig. 12: Compare HDR results on *forrest* of Gallo's [16] dataset with the state-of-the-art methods of Gallo et al. [16], Hu12 et al. [65] and Hu13 et al. [13]

other methods. In addition, the greatest advantage of FBLS is fast training. We compare the training time with Kalantari et al. [14] which cost nearly three days to train their CNN network on Kalantari's dataset, while our FBLS only cost 10 minutes. We firstly input 30 sets of images as the training set, then add 10 sets each time and record the training time. With the increase of the training images, Kalantari's (the traditional deep learning method) training time has significant growth. However, due to our model is a flat network, our training time is much less than deep learning.

VII. CONCLUSION AND FUTURE WORK

In this paper, we propose a novel model in HDR synthesis filed which synthesizes HDR image using a set of multi-view LDR images. For generating high-quality HDR results, we use the fuzzy broad learning system as our learning model and create the dataset of multi-view LDR images with its corresponding ground truth. The training time of our system is much less than the deep neural network since our model is a flat network consisting of fuzzy subsystems and enhancement groups. In addition, we present the incremental learning algorithm for this model. We can increase the enhancement

groups and fuzzy subsystems to optimize our model instead of retraining the whole network. We compare massive substantial experiments with the state-of-the-art methods to prove our results contain more details and less ghosting.

11

However, there are some limitations in our work. Due to the restriction of the model, we could not support multiple input LDRs for more than three images. More LDR images can contain more complete details of the scene. In addition, there are many matrix operations in the computation of weights, which requires lots of memory. Therefore, in the future, we will attempt to optimize our model to support more LDR inputs. And, we will try to reduce the space complexity for the computation of weights.

REFERENCES

- C. Liu, "Beyond pixels: Exploring new representations and applications for motion analysis," Ph.D. dissertation, Massachusetts Institute of Technology, Cambridge, MA, USA, 2009.
- [2] Y. Tao, Y. Shen, B. Sheng, P. Li, and R. W. H. Lau, "Video decolorization using visual proximity coherence optimization," *IEEE Transactions on Cybernetics*, vol. 48, no. 5, pp. 1406–1419, 2018.
- [3] B. Zhang, B. Sheng, P. Li, and T.-Y. Lee, "Depth of field rendering using multilayer-neighborhood optimization," *IEEE Transactions on Visualization and Computer Graphics*, pp. 1–14, 2019.

- [4] B. Sheng, P. Li, S. Mo, H. Li, X. Hou, Q. Wu, J. Qin, R. Fang, and D. D. Feng, "Retinal vessel segmentation using minimum spanning superpixel tree detector," *IEEE Transactions on Cybernetics*, vol. 49, no. 7, pp. 2707–2719, 2019.
- [5] B. Sheng, P. Li, Y. Jin, P. Tan, and T.-Y. Lee, "Intrinsic image decomposition with step and drift shading separation," *IEEE Transactions on Visualization and Computer Graphics*, pp. 1–14, 2018.
- [6] S. K. Nayar and T. Mitsunaga, "High dynamic range imaging: Spatially varying pixel exposures," in *IEEE CVPR*, vol. 1, 2000, pp. 472–479.
- [7] M. McGuire, W. Matusik, H. Pfister, B. Chen, J. F. Hughes, and S. K. Nayar, "Optical splitting trees for high-precision monocular imaging," *IEEE Computer Graphics and Applications*, vol. 27, no. 2, pp. 32–42, 2007
- [8] S. W. Hasinoff, F. Durand, and W. T. Freeman, "Noise-optimal capture for high dynamic range photography," in *IEEE CVPR*, 2010, pp. 553– 560.
- [9] M. D. Tocci, C. Kiser, N. Tocci, and P. Sen, "A versatile HDR video production system," *ACM Transactions on Graphics*, vol. 30, no. 4, pp. 41:1–41:10, 2011.
- [10] P. E. Debevec and J. Malik, "Recovering high dynamic range radiance maps from photographs," in ACM SIGGRAPH, 1997, pp. 369–378.
- [11] S. Mann and R. W. Picard, "Being 'undigital' with digital cameras: Extending dynamic range by combining differently exposed pictures," Massachusetts Institute of Technology, Cambridge, MA, USA, Tech. Rep. 323, 1994.
- [12] P. Sen, N. K. Kalantari, M. Yaesoubi, S. Darabi, D. B. Goldman, and E. Shechtman, "Robust patch-based HDR reconstruction of dynamic scenes," ACM Transactions on Graphics, vol. 31, no. 6, pp. 203:1– 203:11, 2012.
- [13] J. Hu, O. Gallo, K. Pulli, and X. Sun, "HDR deghosting: How to deal with saturation?" in *IEEE CVPR*, 2013, pp. 1163–1170.
- [14] N. K. Kalantari and R. Ramamoorthi, "Deep high dynamic range imaging of dynamic scenes," ACM Transactions on Graphics, vol. 36, no. 4, pp. 144:1–144:12, 2017.
- [15] G. Eilertsen, J. Kronander, G. Denes, R. K. Mantiuk, and J. Unger, "HDR image reconstruction from a single exposure using deep CNNs," ACM Transactions on Graphics, vol. 36, no. 6, pp. 178:1–178:15, 2017.
- [16] O. Gallo, N. Gelfandz, M. Tico, and K. Pulli, "Artifact-free high dynamic range imaging," in *IEEE International Conference on Com*putational Photography, 2009, pp. 1–7.
- [17] Y. S. Heo, K. M. Lee, S. U. Lee, Y. Moon, and J. Cha, "Ghost-free high dynamic range imaging," in *Asian Conference on Computer Vision*, 2011, pp. 486–500.
- [18] T. Mertens, J. Kautz, and F. Van Reeth, "Exposure fusion: A simple and practical alternative to high dynamic range photography," *Computer Graphics Forum*, vol. 28, no. 1, pp. 161–171, 2009.
- [19] C. Lee, Y. Li, and V. Monga, "Ghost-free high dynamic range imaging via rank minimization," *IEEE Signal Processing Letters*, vol. 21, no. 9, pp. 1045–1049, 2014.
- [20] X. Qin, J. Shen, X. Mao, X. Li, and Y. Jia, "Robust match fusion using optimization," *IEEE Transactions on Cybernetics*, vol. 45, no. 8, pp. 1549–1560, 2015.
- [21] K. Ma, H. Li, H. Yong, Z. Wang, D. Meng, and L. Zhang, "Robust multi-exposure image fusion: A structural patch decomposition approach," *IEEE Transactions on Image Processing*, vol. 26, no. 5, pp. 2519–2532, 2017.
- [22] S. Feng and C. L. P. Chen, "Fuzzy broad learning system: A novel neuro-fuzzy model for regression and classification," *IEEE Transactions* on Cybernetics, pp. 1–11, 2018.
- [23] G. Ward, "Fast, robust image registration for compositing high dynamic range photographs from hand-held exposures," *Journal of Graphics Tools*, vol. 8, no. 2, pp. 17–30, 2003.
- [24] A. Tomaszewska and R. Mantiuk, "Image registration for multi-exposure high dynamic range image acquisition," in *International Conference in Central Europe on Computer Graphics*, Visualization and Computer Visio, 2007, pp. 49–56.
- [25] L. Bogoni, "Extending dynamic range of monochrome and color images through fusion," in *International Conference on Pattern Recognition*, vol. 3, 2000, pp. 7–12.
- [26] S. B. Kang, M. Uyttendaele, S. Winder, and R. Szeliski, "High dynamic range video," ACM Transactions on Graphics, vol. 22, no. 3, pp. 319– 325, 2003.
- [27] S. Mangiat and J. Gibson, "High dynamic range video with ghost removal," in *Proc. SPIE*, vol. 7798, 2010.
- [28] H. Zimmer, A. Bruhn, and J. Weickert, "Freehand HDR imaging of moving scenes with simultaneous resolution enhancement," *Computer Graphics Forum*, vol. 30, no. 2, pp. 405–414, 2011.

[29] X. Liu and A. El Gamal, "Synthesis of high dynamic range motion blur free image from multiple captures," *IEEE Transactions on Circuits and Systems I: Fundamental Theory and Applications*, vol. 50, no. 4, pp. 530–539, 2003.

12

- [30] T. Grosch, "Fast and robust high dynamic range image generation with camera and object movement," in *Vision, Modeling and Visualization*, 2006, pp. 1–9.
- [31] S. Raman and S. Chaudhuri, "Reconstruction of high contrast images for dynamic scenes," *The Visual Computer*, vol. 27, no. 12, pp. 1099–1114, 2011.
- [32] E. A. Khan, A. O. Akyuz, and E. Reinhard, "Ghost removal in high dynamic range images," in *IEEE ICIP*, 2006, pp. 2005–2008.
- [33] K. Jacobs, C. Loscos, and G. Ward, "Automatic high-dynamic range image generation for dynamic scenes," *IEEE Computer Graphics and Applications*, vol. 28, no. 2, pp. 84–93, 2008.
- [34] T. Jinno and M. Okuda, "Motion blur free HDR image acquisition using multiple exposures," in *IEEE ICIP*, 2008, pp. 1304–1307.
- [35] Y. Nie, H. Sun, P. Li, C. Xiao, and K.-L. Ma, "Object movements synopsis via part assembling and stitching," *IEEE Transactions on Visualization and Computer Graphics*, vol. 20, no. 9, pp. 1303–1315, 2014.
- [36] Y. Nie, C. Xiao, H. Sun, and P. Li, "Compact video synopsis via global spatiotemporal optimization," *IEEE Transactions on Visualization and Computer Graphics*, vol. 19, no. 10, pp. 1664–1676, 2013.
- [37] D. Sidibe, W. Puech, and O. Strauss, "Ghost detection and removal in high dynamic range images," in *European Signal Processing Conference*, 2009, pp. 2240–2244.
- [38] T.-H. Min, R.-H. Park, and S. Chang, "Histogram based ghost removal in high dynamic range images," in *IEEE ICME*, 2009, pp. 530–533.
- [39] F. Pece and J. Kautz, "Bitmap movement detection: HDR for dynamic scenes," in *Conference on Visual Media Production*, 2010, pp. 1–8.
- [40] S. Wu, S. Xie, S. Rahardja, and Z. Li, "A robust and fast anti-ghosting algorithm for high dynamic range imaging," in *IEEE ICIP*, 2010, pp. 397–400.
- [41] W. Zhang and W.-K. Cham, "Gradient-directed composition of multiexposure images," in *IEEE CVPR*, 2010, pp. 530–536.
- [42] N. K. Kalantari, E. Shechtman, C. Barnes, S. Darabi, D. B. Goldman, and P. Sen, "Patch-based high dynamic range video," *ACM Transactions on Graphics*, vol. 32, no. 6, pp. 202:1–202:8, 2013.
- [43] M. Granados, K. I. Kim, J. Tompkin, and C. Theobalt, "Automatic noise modeling for ghost-free HDR reconstruction," ACM Transactions on Graphics, vol. 32, no. 6, pp. 201:1–201:10, 2013.
- [44] T.-H. Oh, J.-Y. Lee, Y.-W. Tai, and I. S. Kweon, "Robust high dynamic range imaging by rank minimization," *IEEE Transactions on Pattern Analysis and Machine Intelligence*, vol. 37, no. 6, pp. 1219–1232, 2015.
- [45] D. Lin, R. Zhang, Y. Ji, P. Li, and H. Huang, "SCN: Switchable context network for semantic segmentation of RGB-D images," *IEEE Transactions on Cybernetics*, pp. 1–12, 2018.
- [46] A. Kamel, B. Sheng, P. Yang, P. Li, R. Shen, and D. D. Feng, "Deep convolutional neural networks for human action recognition using depth maps and postures," *IEEE Transactions on Systems, Man, and Cybernetics: Systems*, pp. 1–14, 2018.
- [47] A. Kamel, B. Sheng, P. Li, J. Kim, and D. D. Feng, "Efficient body motion quantification and similarity evaluation using 3-D joints skeleton coordinates," *IEEE Transactions on Systems, Man, and Cybernetics:* Systems, pp. 1–15, 2019.
- [48] B. Sheng, P. Li, C. Gao, and K.-L. Ma, "Deep neural representation guided face sketch synthesis," *IEEE Transactions on Visualization and Computer Graphics*, pp. 1–14, 2018.
- [49] E. Shelhamer, J. Long, and T. Darrell, "Fully convolutional networks for semantic segmentation," *IEEE Transactions on Pattern Analysis and Machine Intelligence*, vol. 39, no. 4, pp. 640–651, 2017.
- [50] O. Abdel-Hamid, A.-r. Mohamed, H. Jiang, L. Deng, G. Penn, and D. Yu, "Convolutional neural networks for speech recognition," *IEEE/ACM Transactions on Audio, Speech, and Language Processing*, vol. 22, no. 10, pp. 1533–1545, 2014.
- [51] M. Gong, J. Zhao, J. Liu, Q. Miao, and L. Jiao, "Change detection in synthetic aperture radar images based on deep neural networks," *IEEE Transactions on Neural Networks and Learning Systems*, vol. 27, no. 1, pp. 125–138, 2016.
- [52] W. Hou, X. Gao, D. Tao, and X. Li, "Blind image quality assessment via deep learning," *IEEE Transactions on Neural Networks and Learning Systems*, vol. 26, no. 6, pp. 1275–1286, 2015.
- [53] G. E. Hinton, S. Osindero, and Y.-W. Teh, "A fast learning algorithm for deep belief nets," *Neural Computation*, vol. 18, no. 7, pp. 1527–1554, 2006

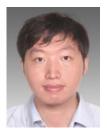
[54] Y. Lecun, L. Bottou, Y. Bengio, and P. Haffner, "Gradient-based learning applied to document recognition," *Proceedings of the IEEE*, vol. 86, no. 11, pp. 2278–2324, 1998.

- [55] M. Leshno, V. Y. Lin, A. Pinkus, and S. Schocken, "Multilayer feedforward networks with a nonpolynomial activation function can approximate any function," *Neural Networks*, vol. 6, no. 6, pp. 861– 867, 1993.
- [56] Y. H. Pao and Y. Takefuji, "Functional-link net computing: theory, system architecture, and functionalities," *Computer*, vol. 25, no. 5, pp. 76–79, 1992.
- [57] Y.-H. Pao, G.-H. Park, and D. J. Sobajic, "Learning and generalization characteristics of the random vector functional-link net," *Neurocomput*ing, vol. 6, no. 2, pp. 163–180, 1994.
- [58] C. L. P. Chen and J. Z. Wan, "A rapid learning and dynamic stepwise updating algorithm for flat neural networks and the application to timeseries prediction," *IEEE Transactions on Systems, Man, and Cybernetics*, Part B (Cybernetics), vol. 29, no. 1, pp. 62–72, 1999.
- [59] C. L. P. Chen and Z. Liu, "Broad learning system: An effective and efficient incremental learning system without the need for deep architecture," *IEEE Transactions on Neural Networks and Learning* Systems, vol. 29, no. 1, pp. 10–24, 2018.
- [60] Z. Chen, T. Gao, B. Sheng, P. Li, and C. L. P. Chen, "Outdoor shadow estimating using multiclass geometric decomposition based on BLS," *IEEE Transactions on Cybernetics*, pp. 1–14, 2018.
- [61] D. Wang, X.-J. Zeng, and J. A. Keane, "Hierarchical hybrid fuzzy-neural networks for approximation with mixed input variables," *Neurocomput*ing, vol. 70, no. 16-18, pp. 3019–3033, 2007.
- [62] H.-J. Rong, G.-B. Huang, N. Sundararajan, and P. Saratchandran, "Online sequential fuzzy extreme learning machine for function approximation and classification problems," *IEEE Transactions on Systems, Man, and Cybernetics, Part B (Cybernetics)*, vol. 39, no. 4, pp. 1067–1072, 2009.
- [63] Z.-L. Sun, K.-F. Au, and T.-M. Choi, "A neuro-fuzzy inference system through integration of fuzzy logic and extreme learning machines," *IEEE Transactions on Systems, Man, and Cybernetics, Part B (Cybernetics)*, vol. 37, no. 5, pp. 1321–1331, 2007.
- [64] R. Mantiuk, K. J. Kim, A. G. Rempel, and W. Heidrich, "HDR-VDP-2: A calibrated visual metric for visibility and quality predictions in all luminance conditions," ACM Transactions on Graphics, vol. 30, no. 4, pp. 40:1–40:14, 2011.
- [65] J. Hu, O. Gallo, and K. Pulli, "Exposure stacks of live scenes with handheld cameras," in *European Conference on Computer Vision*, 2012, pp. 400, 512



Hongbin Guo received the B.Eng. degree in intelligence science and technology from the Sun Yatsen University, Guangzhou, China. He is currently pursuing the M.Eng. degree in computer science with the Department of Computer Science and Engineering, Shanghai Jiao Tong University, Shanghai, China.

His current research interests include high dynamic range image synthesis, fuzzy broad learning system, and computer vision.



Bin Sheng received the Ph.D. degree in computer science and engineering from The Chinese University of Hong Kong, Hong Kong.

He is currently an Associate Professor with the Department of Computer Science and Engineering, Shanghai Jiao Tong University, Shanghai, China. His current research interests include virtual reality, and computer graphics.



Ping Li (M'14) received the Ph.D. degree in computer science and engineering from The Chinese University of Hong Kong, Shatin, Hong Kong.

He is currently a Research Assistant Professor with The Hong Kong Polytechnic University, Kowloon, Hong Kong. He has one image/video processing national invention patent, and has excellent research project reported worldwide by *ACM TechNews*. His current research interests include image/video stylization, artistic rendering and synthesis, and creative media.



C. L. Philip Chen (S'88–M'88–SM'94–F'07) received the M.S. degree in electrical engineering from the University of Michigan, Ann Arbor, MI, USA, in 1985, and the Ph.D. degree in electrical engineering from Purdue University, West Lafayette, IN, USA, in 1988

He is currently a Chair Professor and the Dean of the School of Computer Science and Engineering, South China University of Technology, Guangzhou, China. Being a Program Evaluator of the Accreditation Board of Engineering and Technology E-

ducation (ABET) in the USA, for computer engineering, electrical engineering, and software engineering programs, he successfully architects the University of Macau's Engineering and Computer Science programs receiving accreditations from Washington/Seoul Accord through Hong Kong Institute of Engineers (HKIE), of which is considered as his utmost contribution in engineering/computer science education for Macau as the former Dean of the Faculty of Science and Technology. His current research interests include systems, cybernetics, and computational intelligence.

Dr. Chen was a recipient of the IEEE Norbert Wiener Award in 2018 for his contribution in systems and cybernetics, and machine learning, the 2018 Highly Cited Researcher Award in Computer Science by Clarivate Analytics, the 2016 Outstanding Electrical and Computer Engineers Award from his alma mater, Purdue University, after he graduated from the University of Michigan at Ann Arbor in 1985. He was the IEEE Systems, Man, and Cybernetics Society President from 2012 to 2013, and currently, he is the Editor-in-Chief of the IEEE Transactions on Systems, Man, and Cybernetics: Systems, an Associate Editor of the IEEE Transactions on Fuzzy Systems, and IEEE Transactions on Cybernetics. Currently, he is a Vice President of Chinese Association of Automation (CAA). He is a fellow of AAAS, IAPR, CAA, and HKIE; a member of Academia Europeae, European Academy of Sciences and Arts, and International Academy of Systems and Cybernetics Science.